MHD SIMULATIONS OF DISK-MAGNETIZED STAR INTERACTIONS IN QUIESCENT REGIME: FUNNEL FLOWS AND ANGULAR MOMENTUM TRANSPORT

M.M. Romanova $^1,~{\rm G.V.}$ Ustyugova $^2,~{\rm A.V.}$ Koldoba $^3,~{\rm And}~{\rm R.V.E.}$ Lovelace 4 \$Draft~version~October~27,~2018

ABSTRACT

Magnetohydrodynamic (MHD) simulations have been used to study disk accretion to a rotating magnetized star with an aligned dipole moment. Quiescent initial conditions were developed in order to avoid the fast initial evolution seen in earlier studies. A set of simulations was performed for different stellar magnetic moments and rotation rates. Simulations have shown that the disk structure is significantly changed inside a radius r_{br} where magnetic braking is significant. In this region the disk is strongly inhomogeneous. Radial accretion of matter slows as it approaches the area of strong magnetic field and a dense ring and funnel flow form at the magnetospheric radius r_m where the magnetic pressure is equal to the total, kinetic plus thermal, pressure of the matter.

Funnel flows (FF), where the disk matter moves away from the disk plane and flows along the stellar magnetic field, are found to be stable features during many rotations of the disk. The dominant force driving matter into the FF is the pressure gradient force, while gravitational force accelerates it as it approaches the star. The magnetic force is much smaller than the other forces. The funnel flow is found to be strongly sub-Alfvénic everywhere. The FF is subsonic close to the disk, but it becomes supersonic well above the disk. Matter reaches the star with a velocity close to that of free-fall.

Angular momentum is transported to the star dominantly by the magnetic field. In the disk the transport of angular momentum is mainly by the matter, but closer to the star the matter transfers its angular momentum to the magnetic field and the magnetic field is dominant in transporting angular momentum to the surface of the star. For slowly rotating stars we observed that magnetic braking leads to the deceleration of the inner regions of the disk and the star spins up. For a rapidly rotating star, the inner regions of the disk rotate with a super-Keplerian velocity, and the star spins-down. The average torque is found to be zero when the corotation radius $r_{cor} \approx 1.5 r_m$.

The evolution of the magnetic field in the corona of the disk depends on the ratio of magnetic to matter energies in the corona and in the disk. Most of the simulations were performed in the regime of a relatively dense corona where the matter energy density was larger than the magnetic energy density. In this case the coronal magnetic field gradually opens but the velocity and density of outflowing matter are small. In a test case where a significant part of the corona was in the field dominated regime, more dramatic opening of the magnetic field was observed with the formation of magneto-centrifugally driven outflows.

Numerical applications of our simulation results are made to T Tauri stars. We conclude that our quasi-stationary simulations correspond to the classical T Tauri stage of evolution. Our results are also relevant to cataclysmic variables and magnetized neutron stars in X-ray binaries.

 $Subject\ headings:\ accretion,\ dipole\ --\ plasmas\ --\ magnetic\ fields\ --\ stars:\ magnetic\ fields\ --\ X-rays:\ stars$

1. INTRODUCTION

Disk accretion to a rotating magnetized star is important in a number of astrophysical objects, including T Tauri stars (Edwards *et al.* 1994), cataclysmic variables (e.g., Warner 1995), and X-ray pulsars (e.g., Bildsten *et al.* 1997).

The accretion of matter to a rotating star with a dipole magnetic field is a complicated problem still only partially solved. The important questions which need to be answered include: (1) What is the structure of the disk near the magnetized star? (2) Where is the inner radius of the disk? (3) What is the nature of the funnel flows (FF)? For example, which force is dominant in lifting matter to the

funnel flow? (4) How is the accretion rate influenced by the star's magnetic moment μ and angular velocity Ω_* ? (5) What is the mechanism of angular momentum transport between the star and the disk? What determines whether star spins-up or spins-down? (6) What are the necessary conditions for magneto-centrifugally driven outflows from the disk and/or the star?

Many of these questions have been investigated analytically, but the conclusions reached by different authors often differ because the simplifying assumptions are different. For example, regarding question (2), some authors conclude that the disk should be disrupted in the region where magnetic and matter stresses are comparable (e.g.,

¹Department of Astronomy, Cornell University, Ithaca, NY 14853-6801; Romanova@astrosun.tn.cornell.edu

²Keldysh Institute of Applied Mathematics, Russian Academy of Sciences, Moscow, Russia; Ustyugg@spp.Keldysh.ru

³Institute of Mathematical Modelling, Russian Academy of Sciences, Moscow, Russia; Koldoba@spp.Keldysh.ru

 $^{^4\}mathrm{Department}$ of Astronomy, Cornell University, Ithaca, NY 14853-6801; RVL1@cornell.edu

Fig. 1.— Initial conditions of Types I (left panel) and II (right panel). The gray-scale and numbers show density distribution.

Pringle and Rees 1972 - hereafter PR72; Davidson & Ostriker 1973; Lamb, Pethick & Pines 1973; Ghosh, Lamb, & Pethick 1977; Scharlemann 1978; Ghosh & Lamb 1979 a,b - hereafter GL79a,b; Camenzind 1990; Königl 1991; Shu it et al. 1994 - hereafter S94). Others, argue that the inner radius of the disk should be farther away, at the corotation radius, because the inner regions of the disk are disrupted by magnetic braking (Ostriker & Shu 1995 - hereafter OS95; Branderburg & Campbell 1998; Elstner & Rüdiger 2000).

Question (3) is investigated in only a few papers which use the Bernoulli integral (Lamb, Pethick & Pines 1977; Paatz & Camenzind 1996 – hereafter PC96; Li & Wilson 1999; and Koldoba et al. 2002). The authors agree that the flow should become supersonic (and slow magnetosonic) just above the disk. On the other hand opinions differ regarding the driving force which pushes matter up into the FF. Li and Wilson (1999) (see also Li et al. 1996) propose that the twisting of the magnetic field near the base of the FF should be very large, $\gamma_{\phi} = |B_{\phi}|/B_p >> 1$ and the magnetic force should be the main one lifting matter to the FF. Here, B_{ϕ} is the toroidal component of the magnetic field and B_p is the poloidal component. Other groups (e.g., Lamb et al. 1977; PC96; Koldoba et al. 2002) argue that the FF should be super-Alvénic so that the twisting of the field is small so that the magnetic force is also small. In numerical simulations by MS97, H97 and GBW99 the magnetospheric accretion was reported, but no clear evidence of funnel flows was presented and no analysis of FFs was performed. A significant part of this paper is devoted to the FFs. Another important issue which has been discussed over the past 30 years is question (5) concerning the transport of angular momentum between the disk and the star. What determines the sign of the torque on the star? In early papers it was supposed that a star can only be spun-up because matter in a Keplerian disk brings positive angular momentum to the star (e.g., PR72). Later, it was recognized that a star can be spun-down due to the part of the star's magnetic flux which passes through the disk outside of the corotation radius (GL79b, Wang 1995). Recently, the idea of "torqueless" accretion was proposed where mass but not angular momentum is transported to a star (e.g. S94; OS95; Li, Wickramasinghe & Rüdiger 1996; Li & Wickramasinghe 1997). Wang (1997) presented arguments against this idea, but this still remains an open question.

Question (6) regarding magneto-centrifugally driven outflows from the disk has been discussed by a number of authors (e.g., Camenzind 1990; Königl 1991; S94; OS95; Lovelace, Romanova & Bisnovatyi-Kogan 1995 - hereafter LRBK95; Fendt, Camenzind & Appl 1995; PC96; Goodson & Winglee 1999; Bardou & Heyvaerts 1999; Agapitou & Papaloizou 2000). For example, S94 proposed that poloidal magnetic flux accumulates near the corotation radius and magnetic winds should blow from this point (X-point). LRBK95 proposed that wind may form from the entire region of the disk outside the corotation radius where the magnetic field threading the disk is open.

Analytical investigations of disk accretion to a magnetized star are of course limited by the different assumptions made. For this reason robust 2D and 3D simulations are essential to further the understanding of the different phenomena. By robust we mean that the result should not depend on initial conditions, boundary conditions, on grid resolution, and other artificial factors. Several 2D MHD simulation studies have been made with different initial conditions aimed at disk/star outflows. In an early work Hayashi, Shibata, and Matsumoto (1996) (hereafter HSM96) investigated the interaction of a non-rotating star with a Keplerian accretion disk and observed the opening of magnetic field lines which initially thread both the star and the disk. They found single event outflows and the corresponding inward collapse of the disk on a dynamical time-scale (less than one period of rotation of the inner radius of the disk) with the radial velocity of the disk close to free-fall. This fast evolution was the result of the magnetic braking of the disk by the magnetic field linking the disk and non-rotating star through a conducting corona. This explosive behavior may correspond to some episodic accretion events of actual systems. However, it is important to investigate the possible quiescent behavior of the disk-star systems.

Miller and Stone (1997; hereafter MS97) investigated disk-star interaction for different geometries and stellar magnetic fields using the resistive ZEUS code. MS97 rotated the corona - which occupies all the space between the star and the disk - with the rotation rate of the star. This decreased the initial magnetic braking (compared to HSM96), so that they were able to perform simulations for several periods of rotation of the inner radius of the disk. In cases with a relatively weak magnetic field, they got results similar to those of HSM96. They also found the disk collapsing to the star with velocity $\sim 0.5v_{ff}$, the opening of magnetic field lines, and outflows of matter from the disk. However, in the case of a strong magnetic field, particularly in the case which included a uniform homogeneous vertical magnetic field threading the disk, they observed diminished outflows. Instead the matter flowed around the magnetosphere to the star. Similar results were obtained by Hirose et al. (1997; hereafter H97).

Goodson, Winglee and Böhm (1997) (hereafter GWB97) and Goodson, Böhm and Winglee (1999) (hereafter GBW99) did much longer simulations in very large simulation regions. They observed quasi-periodic matter outbursts associated with the quasi-periodic opening of magnetic field lines and matter accretion to the star. The density in the corona was chosen to decrease in a special way, $1/R^4$, so that the Alfvén speed $\propto B/\sqrt{\rho} \propto 1/R$ decreases gradually. This is favorable for the opening of magnetic field lines, and for the generation and propagation of outflows. GWB97 and GBW99 do not investigate cases where the density falls off more slowly with distance.

Fendt and Elstner (1999, 2000 – hereafter FE99, FE00) investigated disk-star interaction for thousands of rotations of the inner radius of the disk, and observed the opening of magnetic field lines and outflows. However,

Fig. 2.— Evolution of a disk with no magnetic field for initial conditions of Type I (panels a, b, c, d) and Type II (panels e, f, g, h). Panels a & e show initial density distribution. Other panels show density distribution for different viscosities, $\alpha=0,\ 0.01,\$ and 0.02 at T=50. The initial density for initial conditions of Type II is about 1.5 times smaller than for Type I. Consequently the density scale is slightly different in these cases. The legend for ρ is chosen to show the density distribution in the main part of the disk. It does not reflect the low density in the corona where $\rho_{min}=0.003$ and the highest densities of matter in the disk near the star where $\rho_{max}=18$ at the panel $c,\ \rho_{max}=12$ at the panel $d,\ \rho_{max}=2.1$ at the panel $d,\ \rho_{max}=4.2$ at the panel $d,\ \rho_{max}=4.2$ at the panel $d,\ \rho_{max}=4.2$

Fig. 3.— Evolution of the disk and the poloidal magnetic field in the largest region studied, $R_{max} = 55$. The density (gray scale background) varies from a minimum value $\rho = 0.003$ in the corona to a maximum value $\rho = 2.6$ in the disk. The field lines are labelled by their magnetic flux Ψ values which change from 0.0009 to 4.9.

Fig. 4.— Evolution of the disk and the magnetic field in a medium size region $R_{max}=7$. The configurations at T=0,10,20,30,40,&50 are shown. The density (gray scale background) changes from maximum value $\rho=2.6$ in the disk to the minimum value $\rho=0.003$ in the corona. Contour levels of Ψ , which label poloidal field lines, change from 4.9 to 0.006. The field lines of the strongest magnetic field near the star are not included in order to make the inner structure of the disk visible.

they treated the disk as a boundary condition so that they could not take into account the back reaction of the disk on the stellar magnetic field. Furthermore, the actual outflow of matter from the disk to the corona may be different from that assumed.

The above – mentioned simulation studies show that outflows appear either in very non-stationary situations (HSM96, MS97) or for a special distribution of coronal density and very fast rotation of the star (GWB97, GBW99). None of the papers give answer to questions (1)-(5). Also, it is not clear whether or not outflows exist for more quiescent initial conditions, and for cases where the coronal density falls off slowly with distance.

In this paper we investigate disk accretion to a rotating magnetized star and the associated funnel flows. We start from initial conditions which give us the possibility to significantly reduce the initial magnetic braking between the disk and the corona. This allows us to investigate the disk-star interaction and funnel flows for long times and to consider questions (1)-(5) in detail.

In §2 we describe the numerical model, including initial and boundary conditions. We also discuss the evolution of the disk without a magnetic field. In §3 we describe in detail the disk-star interaction for the case of slowly rotating stars and in §4 cases of fast rotating stars. In §5 we consider the dependence of disk-star interaction on the magnetic moment μ . In §6 we analyze the physics of FFs. In §7 we consider the possibility of outflows. In §8 we apply our simulation results to T Tauri stars. In §9 give the conclusions from this work.

2. NUMERICAL SIMULATIONS

To investigate the disk-star interaction, we numerically solve the MHD equations,

$$\frac{\partial \rho}{\partial t} + \nabla \cdot (\rho \mathbf{v}) = 0 \quad (1), \quad \frac{\partial (\rho \mathbf{v})}{\partial t} + \nabla \cdot \mathcal{T} = \rho \mathbf{g}$$
 (2)

$$\frac{\partial \mathbf{B}}{\partial t} - \nabla \times (\mathbf{v} \times \mathbf{B}) = 0 \quad (3), \quad \frac{\partial (\rho S)}{\partial t} + \nabla \cdot (\rho \mathbf{v} S) = 0 \; . \; (4)$$

Here, S is entropy, $\mathcal{T}_{jk} = p\delta_{jk} + \rho v_j v_k + (\mathbf{B}^2 \delta_{jk}/2 - B_j B_k)/(4\pi)$ is the stress tensor, $\mathbf{g} = -\nabla \Phi$ is the gravitational acceleration, and $\Phi = -GM/R$ is the gravitational

potential of the central object. We take the equation of state to be $S = p/\rho^{\gamma}$, where $\gamma = 5/3$ for most of this work. We solve equations (1)-(4) in a spherical coordinate system (R, θ, ϕ) .

In order to model the slow accretion of matter in the disk we modified equations (2) and (4) by including a small viscous stress σ_{jk} in \mathcal{T}_{jk} . Because the flow is dominantly in the azimuthal direction the main viscous stress acts in this direction. Thus the important viscous stress components are the $(R\phi)$ and $(\theta\phi)$ terms, $\sigma_{R\phi} = -\nu\rho R\sin\theta\partial\omega/\partial R$, $\sigma_{\theta\phi} = -\nu\rho\sin\theta\partial\omega/\partial\theta$, where $\omega = v_{\phi}/R\sin\theta$ is angular velocity of the matter, and ν is the kinematic viscosity. We adopt the α - model for the viscosity (Shakura & Sunyaev 1973), where $\nu = \alpha c_s^2/\Omega_K$, with $c_s = (p/\rho)^{1/2}$ the isothermal sound speed velocity and $\alpha \ll 1$ is a dimensionless parameter, which was chosen to be $\alpha = 0.01$ or $\alpha = 0.02$ in most of simulations which gave a reasonable speed of matter flow to the central regions. We checked that for the grid sizes used the numerical viscosity is much lower than the considered α viscosity (see §2.5).

Equations (1) - (4) were solved with a Godunov type numerical code developed and tested by Koldoba et al. (1992), Koldoba and Ustyugova (1994) and Ustyugova et al. (1995). This type of code has also been described by Ryu, Jones, and Frank (1995). A modified version of the code incorporating viscosity was tested in a number of hydrodynamic simulations for different values of α , from $\alpha = 0.01$ to $\alpha = 0.1$. For $\alpha \sim 0.01 - 0.05$ we observed a steady flow of matter to the star with small velocities (see §2.5) corresponding approximately to the Shakura-Sunyaev accretion model.

Our Godunov type code does not explicitly include magnetic diffusivity (unlike the codes of MS97, H97, & GBW99). However, matter diffuses across the magnetic field owing to the small numerical diffusivity ν_m which is of the order of the numerical viscosity $\nu_m \sim \Delta R c_s$, where ΔR is the grid spacing. The estimated magnetic Reynolds number associated with the radial flow is $Re_m \sim \delta R v_r / \nu_m$, where δR is the characteristic scale. In the region 1 < R < 5, $Re_m \sim 3$ owing to the small radial velocity v_r . In actual accretion disks, both angular momentum transport and diffusion of the magnetic field, are probably due

Fig. 5.— Evolution of the density in the disk (color background) and poloidal magnetic field lines (Ψ =const lines) (white lines) in case of Type I initial conditions in the region r < 6. The black solid line corresponds to $\tilde{\beta} = 1$. The density changes from 0.003 in the corona to 2.4 in the disk. Contours of Ψ are exponentially spaced between 0.2 and 1.2.

Fig. 6.— Same as on Figure 4 but for initial conditions of Type II. At T=0 the inner radius of the disk is at $r=r_{cor}=3$. The Ψ =const lines are exponentially spaced between 0.1 and 0.7.

to turbulence (e.g., Bisnovatyi-Kogan & Ruzmaikin 1976; Balbus & Hawley 1991) and have similar order of magnitude transport coefficients. In our simulations we observed that both the viscosity and the magnetic diffusivity are small and are of the same order of magnitide. Note, that in the ϕ direction, the velocity of the flow is high, and the Reynolds number is also high, $(Re_m)_{\phi} \sim 100$, so that magnetic field lines rotate with the disk in ϕ direction, and at the same time matter slowly diffuses in r-direction. This is important for understanding of evolution of magnetic field lines observed in the following sections.

2.1. Reference Values and Dimensionless Units

A reference value of distance is denoted R_0 . The reference value for velocity is taken to be $v_0 = (GM/R_0)^{1/2}$ which is the Keplerian velocity at R_0 . The reference angular rotation rate is $\omega_0 = v_0/R_0$, and the corresponding time-scale is $t_0 = R_0/v_0$. For discussing our results we also use the rotation period at $r = R_0$, $P_0 = 2\pi t_0$. For a given magnetic field strength at R_0 we can define a reference density as $\rho_0 = B_0^2/v_0^2$ and reference pressure $p_0 = \rho_0 v_0^2$. A reference magnetic moment of the star is then $\mu_0 = B_0 R_0^3$. Thus, the calculated variables are: $R' = R/R_0$, $t' = t/t_0$, $\rho' = \rho/\rho_0$, $v' = v/v_0$, $B' = B/B_0$, $p' = p/p_0$. We also use the dimensionless time, $T = t/P_0$. Later, we omit the primes but note that any dimensionless variable can readily be converted to its physical value.

Here, we give parameters for a typical T Tauri star. We take the mass and radius of the star to be $M_*=0.8M_\odot$ and $R_*=2R_\odot$. We use as the length scale R_0 the initial inner radius of the disk, so that the dimensionless inner radius of the disk is $R_d=1$ in most of simulations. We place the inner boundary (a star) at $R_{min}=0.35$. Then, our reference length is $R_0\approx R_*/0.35\approx 4.0\times 10^{11}$ cm, while the simulation region corresponds to $R_{max}=55\times R_0\approx 1.47$ a.u..

The reference velocity is $v_0 \approx 1.63 \times 10^7$ cm/s, and the corresponding time-scale is $t_0 \approx R_0/v_0 \approx 2.45 \times 10^4$ s. The period of rotation of the inner radius of the disk is $P_0 \approx 1.78$ days.

Consider a magnetic field strength $B_*=10^3$ G at the star's surface. Then at $R=R_0$, the reference magnetic field is $B_0=B_*(R_*/R_0)^3\approx 42.9$ G and the reference magnetic moment is $\mu_0=B_0R_0^3\approx 2.7\times 10^{36}$ Gcm³. The reference density is $\rho_0=6.9\times 10^{-12}$ g/cm³, or $n=6.93\times 10^{12}$ cm⁻³ which is typical for T Tauri star disks. The reference mass accretion rate is $\dot{M}_0=\rho_0v_0R_0^2\approx 1.8\times 10^{18}$ g/s $\approx 2.8\times 10^{-7}$ M_☉/year. The reference angular momentum flux is: $\dot{L}_0=\rho_0v_0^2R_0^2$.

2.2. The Grid

We place the inner boundary of the simulation region the "star" - at $R_{min} = 0.35$. The size of external boundary depends on the grid (see below). The spherical grid was inhomogeneous in the R-direction. The inhomogeneity was such that cells at any distance R were approximately square with $\Delta R \sim R\Delta\theta$ for fixed $\Delta\theta$. This grid gives a high space resolution close to the star which is important in this problem. At the same time simulations in very large regions may be performed. The inhomogeneous grid is a smooth analog of the nested grids used by GBW97 and GBW99.

The angular grid was taken to have $N_{\theta} = 51$ in most cases, and $N_{\theta} = 71$ in cases with very strong magnetic field (see $\S 7$). The number of points in the R-direction determined the size of the simulation region. The main runs were done with a large radial grid $N_R = 150$ which corresponds to $R_{max}=55\approx 157 R_{min}$. Simulations with a smaller grid $N_R=100$ corresponding to $R_{max}=10\approx$ $35R_{min}$ were done in a number of cases. The large size of the region was chosen in order to minimize the influence of external boundaries on processes in the vicinity of the star. We checked, however, that results of simulations in the larger region almost coincide with those in the smaller region. For the typical grid with $N_{\theta} = 51$, the smallest cell near the star corresponds to $\Delta R = 0.01 \approx 0.03 R_{min}$ which is a resolution about 3.2 times higher than one in GBW99. The largest grid is at the external boundary, for $N_R = 150$ and is $\Delta R = 5.4 R_{min}$. These numbers show that a spherical stretched grid is advantageous for simulations of accretion flow to a star with a dipole field.

2.3. Boundary Conditions

At the inner boundary $R = R_{min}$, we apply "free" boundary conditions for the density, pressure, and entropy, $\partial \rho/\partial R = 0$, $\partial \rho/\partial R = 0$, and $\partial S/\partial R = 0$. The inner boundary is treated as a rotating perfect conductor $\Omega = \Omega \hat{\mathbf{z}}$, which is analogous to the case of a rotating disk discussed earlier by Ustyugova et al. (1995, 1999). In the reference frame rotating with the star, the flow velocity ${\bf v}$ is parallel to **B** at $R = R_{min}$; that is, $\mathbf{B} \times (\mathbf{v} - \mathbf{\Omega} \times \mathbf{R}) = \mathbf{0}$ at R_{min} . We consider the "free" boundary condition for this velocity, $\partial (\mathbf{v} - \mathbf{\Omega} \times \mathbf{R})_R / \partial R = 0$. These two conditions determine the direction and value of the velocity vector \mathbf{v} , that is all three components (v_R, v_θ, v_ϕ) . The boundary condition at R_{min} on the magnetic field has $\partial (RB_{\phi})/\partial R=0$, while the poloidal components B_R and B_{θ} are derived from the magnetic flux function $\Psi(R,\theta)$, where Ψ at the boundary is derived from the frozen-in condition $\partial \Psi / \partial t + \mathbf{v}_p \cdot \nabla \Psi = 0$.

At the outer boundary $R = R_{max}$, we took fixed boundary conditions for all variables for those cases when the simulation region was very large: $R_{max} = 55$. In case of smaller region $R_{max} = 10$ we took free boundary conditions on all the hydrodynamic variables and the B_{ϕ} component of the magnetic field, if matter outflows from the region. For the magnetic field we took $\partial B_{\phi}/\partial R = 0$ and

 $\partial \Psi/\partial t + \mathbf{v}_p \cdot \nabla \Psi = 0$. If matter inflows to the region $(v_R(R_{max}) < 0)$, then we set this velocity equal to zero. Results are very similar at these boundary conditions. We assume reflection symmetry about the equatorial plane.

2.4. Initial Conditions

Here we present our new method for establishing quasiequilibrium initial conditions. The star has a magnetic dipole field with the magnetic moment μ aligned with the rotation axis \hat{z} , with Ω_* the star's rotation rate. The magnetic field is $\mathbf{B} = 3(\mu \cdot \mathbf{R})\mathbf{R}/R^5 - \mu/R^3$, with components in spherical coordinates $B_R = 2\mu\cos\theta/R^3$ and $B_\theta = \mu\sin\theta/R^3$. As initial conditions we set up a lowtemperature T_d disk with a high-temperature $T_c \gg T_d$ corona filling the remainder of the simulation region. The disk rotates with angular velocity close to the Keplerian value $\omega \approx \Omega_K$. The disk extends inward to the radius R_d where the ram pressure of the disk is equals to the magnetic pressure of the dipole, $p + \rho \mathbf{v}^2 = B^2/8\pi$.

In order to have approximately equilibrium initial conditions it is necessary that the corona initially be rotating. If the corona initially does not rotate (e.g., HSM96), or rotates with the angular velocity of the star (e.g. MS97), while the disk rotates with Keplerian velocity, then the coronal magnetic field lines threading the disk and the star lead to magnetic braking of the disk and subsequent fast accretion of the disk with a velocity close to free-fall. Furthermore, a strong discontinuity develops in the angular velocity between the disk and the corona (except at the corotation radius). This leads to the generation of a strong B_{ϕ} component, while the dragging of the magnetic field with the radial inflow of the disk leads to the generation of a B_r component. This twisting of the field is responsible for transient magneto-centrifugally driven outflows (e.g HSM96; MS97; Hirose et al. 1997). Such fast evolution may correspond to periods of violent accretion in some strongly non-stationary systems. However, the stardisk systems may exist in more quiescent configurations which can be studied by using appropriate initial condi-

In order to avoid the strong discontinuity of ω and B_{ϕ} on the boundary between the disk and the corona, we rotate the initial corona so that its angular velocity is a constant on a given cylindrical radius $r = R \sin \theta$ and equal to the Keplerian rotation rate of the disk. Thus the corona rotates with different angular velocities on cylinders with different radii r. For such initial conditions we observe much slower accretion in the disk with no dramatic outflows. This distribution of ω in the corona also leads to the twisting of the magnetic field lines. Any coronal magnetic field line will be twisted along its length by the differential rotation of nearby layers of corona, but this twist is distributed along the length of the field line. At the boundary between the disk and corona the twist is small. It is much smaller than the twist at the boundary between a rotating disk and non-rotating corona. Differentially rotating corona also leads to the magnetic braking of the disk, but it is more gradual and does not lead to a rapid infall of the matter in the disk. Earlier, a differentially rotating corona was used as an initial condition in a study of the opening of magnetic loops threading a Keplerian disk, but the disk was considered as a boundary condition (Romanova *et al.* 1998).

Initially, we assume that $B_{\phi}=0$ everywhere. Also, we assume that the initial poloidal field is that of a dipole and that the plasma is force-free. Thus, we search for equilibrium initial conditions for the disk-corona system taking into account gravity, pressure, and rotation. To find the initial equilibrium, we suppose that initially (t=0) the matter is barotropic $\rho=\rho(p)$. In this case one have (1) $\nabla p/\rho=\nabla F$, where $F=\int dp/\rho$; (2) the angular velocity ω depends only on $r=R\sin\theta$; (3) the centrifugal force has the potential $\Phi_c=-\int_{-\infty}^{r}[\omega(r')]^2r'dr'$; (4) the stationary Euler equation $(\mathbf{v}\cdot\nabla)\mathbf{v}+p/\rho+\nabla\Phi=0$ has the integral:

$$F + \Phi_c + \Phi = E = \text{const}, \tag{5}$$

where $\Phi = -GM/R$ is the gravitational potential.

We suppose that the initial angular velocity of the matter in the equatorial plane is

$$\omega(r,\theta = \pi/2) = \begin{cases} (kGM/R_d^3)^{\frac{1}{2}}, & r \le R_d \\ (kGM/r^3)^{\frac{1}{2}}, & r \ge R_d \end{cases}$$
(6)

where $r = R \sin \theta$ is the cylindrical radius, and $k = \text{const} \sim 1$ is included to take into account that the disk is slightly non-Keplerian (in our simulations k = 1.01). Thus, the centrifugal potential in the whole region is

$$\Phi_c(R,\theta) \!=\! \left\{ \! \begin{array}{ll} k(GM/R_d)[1+(R_d^2-r^2)/2R_d^2] \;, & r \leq R_d \\ kGM/r \;, & r \geq R_d \;. \end{array} \right. \label{eq:phicond}$$

At the boundary between the disk and corona the initial pressure is taken to be p_0 . The dependence of the density on pressure in the corona and in the disk can be expressed as

$$\rho(p) = \begin{cases} \bar{m}p/T_c , & p < p_0 \\ \bar{m}p/T_d , & p > p_0 , \end{cases}$$
 (8)

where \bar{m} is the mean particle mass approximately equal to $m_H/2$. We consider that $T_d \ll T_c$. In the corona, at low values of pressure and density $(p < p_0, \rho < \bar{m}p_0/T_c)$ the plasma is hot $T = T_c$, whereas in the disk, at high pressure and density $(p > p_0, \rho > \bar{m}p_0/T_d)$ the plasma is at a much lower temperature, $T = T_d$. Initially, the boundary between the disk and corona corresponds to the contact discontinuity, where $p = p_0$, $\rho_c = \bar{m}p_0/T_c$ in the corona, and $\rho_d = \bar{m}p_0/T_d$ in the disk. In this case

$$F = \begin{cases} (T_c/\bar{m})\ln(p/p_0) , & p \le p_0 \\ (T_d/\bar{m})\ln(p/p_0) , & p \ge p_0 \end{cases} . \tag{9}$$

The initial disk-corona boundary in the equatorial plane is assumed to be at $r = R_d$. We assume values of p_0 , T_c , and T_d . At the point $(r = R_d, z = 0)$, $p = p_0$, $F(p_0) = 0$. Thus, we find $E = -GM/R_d + kGM/R_d = (k-1)GM/R_d$. Then, we can calculate potential $\Phi + \Phi_c$ at any point (R, θ)

Fig. 8.— Distribution of angular velocity in the disk and corona at different times T for the same case as Figures 4 and 5. Only the inner region of the disk r < 4 is shown. ω changes from $\omega = 0.1$ (white) to $\omega = 1$ (black). The solid lines are poloidal field lines (Ψ =const lines).

and find $F = E - (\Phi + \Phi_c)$. Now, we can derive pressure p at any point of the region,

$$p = \begin{cases} p_0 \exp(F\bar{m}/T_c), & p \le p_0 \\ p_0 \exp(F\bar{m}/T_d), & p \ge p_0 \end{cases}$$
 (10)

and find the distribution of density taking into account eq. (8). We considered two main types of initial conditions which are described below.

2.4.1. Initial Conditions of Type I

In the first type of initial conditions, we place the inner radius of the disk at $r = R_d = 1$. We determine the characteristic density and temperature in the corona to be $\rho_c = 0.01, T_c = 1$, and density in the disk $\rho_d = 1$. Then we determine the pressure at the boundary between the disk and corona, $p_0 = \rho_c T_c = 0.01$ and then derive temperature in the disk, $T_d = p_0/\rho_d = 0.01$, so that the pressure is continuous across the boundary. Then we determine the magnetic field of the star so as to have the magnetic pressure equal to the stagnation pressure of the disk matter at R=1. This gives $\mu^2/8\pi R_d^6\approx \rho_d v_K^2$ which is solved for μ . As matter in the disk flows inward, it forms a funnel flow at $R \approx 1$. We determine $\omega(r)$ from equation (6) taking into account that $R_d = 1$. For $r < R_d$ matter rotates with an angular velocity corresponding to $\omega_K(r=1)$, while at $r > R_d$ the rotation is Keplerian. The surfaces of constant ω are cylinders. For such a distribution, there are no strong gradients of ω in the region. Then we derive the pressure and density distributions using equations (5)-(10).

The left panel of Figure 1 shows the density distribution in the disk and corona. For this example we took a relatively small region $R_{max} = 7$. One can see that the density is high in the disk, and is 100 - 200 times smaller in the corona. For these initial conditions the FF starts close to the initial inner radius of the disk. Thus the disk provides a "reservoir" of matter for the FF. On the other hand there is the following disadvantage. In most cases, we rotate the star with an angular velocity Ω_* smaller than the initial angular velocity of matter above the star. Fortunately, the star is observed to control the rotation of the nearby regions of corona in a few time-steps. We also used initial conditions of Type II, as described below.

2.4.2. Initial Conditions of Type II

In a second type of initial conditions we place the inner radius of the disk R_d at the corotation radius, $r_{cor} = (GM/\Omega_*^2)^{1/3}$. Thus for $r < R_d$ both the star and the corona rotate with the angular velocity $\Omega_K(r = R_d)$, while

at larger distances the rotation is Keplerian. For this initial condition, ω varies smoothly including the variation from the star and to the corona above it.

An important aspect of the Type II initial conditions is that the initial inner radius of the disk is far from the magnetosphere. This allows us to check whether or not matter moves inward from the corotation radius.

The left panel of Figure 1 shows the initial density distribution for Type II initial conditions for $r_{cor} = 3$.

2.5. Hydrodynamic Evolution of the Disk and Corona

First, we tested our initial conditions with no magnetic field. We observed that for both types of initial conditions the disk exists for more than 300 rotational periods P_0 . No high velocities appear in the disk or corona. Typical velocities in the disk are $v_d \sim 0.01-0001$. However, our typical time of simulation of magnetic cases is shorter: $50P_0$, so that we show the result of the evolution of the disk without a magnetic field at $t < 50P_0$.

We considered three cases, with no viscosity, $\alpha=0$, and with small viscosities $\alpha=0.01$ and $\alpha=0.02$. Figure 2 (a,b) shows that at $\alpha=0$ and boundary conditions of Type I, the disk's inner edge stays at r=1 during the whole period of evolution. The density in the rest of the disk slowly redistributes itself in such way that the external layers move gradually outward. The outer regions of the disk had excess angular momentum compared to a stationary α -disk (Shakura & Sunyaev 1973), and consequently some matter moved outward carrying away extra angular momentum. When we included a small viscosity $\alpha=0.01$ (see panel c of Figure 2), the outer regions of the disk also moved outward, but inside the shown region r<10 matter moves inward with velocity v<0.0001-0.001 for r>6, and with larger velocity $v\sim0.003-0.006$ for r<6.

For even higher viscosity $\alpha=0.02$ (panel d of Figure 2), the velocity of the inflow is $v\sim 0.003-0.006$ in the entire disk, r<10. In both initial conditions we find that the α -viscosity gives a slow accretion and thus a good starting point for our MHD simulations. The typical accretion rate is $\dot{M}\approx 0.05$ for $\alpha=0.01$ and $\dot{M}\approx 0.1$ for $\alpha=0.02$.

For the Type II initial conditions we observed that for $\alpha=0$ the inner radius of the disk stays at r=3 for T=50. This shows that the numerical viscosity is very small (see panels e and f of Figure 2) compared with an $\alpha=0.01$ viscosity. External regions moved outward with velocity v<0.001, redistributing density and angular momentum. For $\alpha=0.01$ and 0.02, the disk behaved similarly to one for initial conditions of Type I: the equatorial regions accreted slowly inward with velocity $v\sim0.003-0.007$ (panels g and h of Figure 2). The accretion rate is $\dot{M}\approx0.02$ for $\alpha=0.01$ and $\dot{M}\approx0.05$ at $\alpha=0.02$. These tests

Fig. 9.— The figure shows the time dependence of the mass accretion rate \dot{M} and the angular momentum fluxes carried by matter \dot{L}_m and magnetic field \dot{L}_f to the star for the case of a slowly rotating star $\Omega_* = 0.19$ which corresponds to $P_* = 9.4$ days). The corotation radius is $r_{cor} = 3$.

Fig. 10.— Same as on Figure 9, but for initial conditions of Type II.

Fig. 11.— Results of simulations of disk-star interaction for the case of a rapidly rotating star, $\Omega_* = 1$ and $r_{cor} = 1$, which corresponds to $P_* \approx 1.8$ days for the T Tauri parameters of §2.2. The density (background) and poloidal magnetic field lines or Ψ =const lines (solid lines) are shown. The Ψ contours are exponentially spaced between 0.15 and 1.

Fig. 12.— Same as on Figure 9, but $\Omega_* = 1$ and $r_{cor} = 1$ ($P_* = 1.8$ days for the T Tauri parameters of §2.2).

indicate that our hydrodynamic disk and corona are appropriate for subsequent MHD simulations of the disk-star interaction.

Note, that subsequently we observed that accretion rate to the star in the magnetic case is larger than in hydro case (see Figures 9 and 10, where accretion rate is $\dot{M}\approx 0.2-0.4$ at initial conditions of Type I, and $\dot{M}\approx 0.5-1.3$ at initial conditions of Type II, which is connected with small magnetic braking of matter in the disk, because initial conditions give only approximate but not exact initial equilibrium.

3. DISK-STAR INTERACTION FOR A SLOWLY ROTATING STAR

Here, we discuss simulations of accretion to a slowly rotating star with $\Omega_* = 0.19$ ($r_{cor} = 3$), which corresponds to a period $P_* = P_0/\Omega_* \approx 9.4$ days for a typical T Tauri star (see §2.2). The magnetic moment is $\mu = 1.06$, which corresponds to a magnetic field at the surface of the star $B_* \approx 1100$ G. We used initial conditions of Types I and II to check for the possible dependence of the evolution on initial conditions. The simulations were performed with the grid $N_R \times N_\theta = 150 \times 51$ which has $R_{max} = 55$.

3.1. Simulations with Type I Initial Conditions: Structure of the Disk

First, we describe results of simulations with Type I initial conditions. We observed that matter started to move slowly both in the disk and corona with velocities much smaller than free-fall. No dramatic collapse of the disk or fast outflows were observed owing to our quasi-equilibrium initial conditions.

Figure 3 shows the entire simulation region at different times. The outer part of the disk changes very little during the simulation time $T \leq 50$. The magnetic field lines twist and become partially open. Viewed on this large scale, the disk is relatively flared, but only the much smaller region of the disk $R \leq 10$ is important for disk-star interactions.

Figure 4 shows the evolution in the smaller region $R \leq 7$. One can see, that the inner region of the disk is influenced by the magnetic field of the star. For $T \approx 50$ the accretion rate due to the $\alpha-$ viscosity increased and magnetic flux was accumulated in the central region. We stopped the simulations at this point, because later the accretion rate increased, the inner radius of the disk moved closer to the star, and the case became less interesting for the investigation of the disk-star interaction.

Figure 5 shows the evolution of the density and poloidal magnetic field in the region $r \leq 6$. The interaction of the disk with the magnetosphere of the star led to the reconstruction of the disk inside the radius which we call the "braking" radius r_{br} . In this case $r_{br} \approx 3$. This radius is

an approximate analog of the radius of the outer transition zone in the theory of GL79b, which divides areas of an undisturbed viscous disk and inner regions, influenced by a magnetic field. In our case, the disk for $r > r_{br}$ is also disturbed by the star's field, but matter still moves to this region due to viscosity. At smaller radii $r \lesssim r_{br}$, matter is magnetically braked. By coincidence $r_{br} \approx r_{cor}$. The inner regions of the disk become magnetically braked after several rotation periods P_0 . In the region of the magnetic braking the density in the disk is 2-4 times smaller than in the disk without a magnetic field. The inflow speed of the matter increases to $v \sim 0.01 - 0.06$. and matter constantly moves in the direction of the star. The flow towards the star stops when the matter stress becomes comparable to the magnetic pressure of the dipole, $B^2/8\pi = p + \rho v^2$. Note that the main term in the matter stress, ρv_{ϕ}^2 , is due to the disk's rotation. We introduce the plasma parameter, $\tilde{\beta} \equiv (p + \rho v^2)/(B^2/8\pi)$, which indicates the relative importance of the matter and magnetic stresses. Also, we introduce the magnetospheric radius,

$$r_m = \frac{\mu^{1/3}}{[8\pi(p + \rho v^2)]^{1/6}} , \qquad (11)$$

which is the radius at z = 0 where $\beta = 1$.

Figure 5 shows that matter accumulates in the region $r \approx r_m$ forming a dense ring. The density in the ring is $\sim 2-3$ times larger than the initial density at the inner radius of the disk. At T=50, when more matter comes from the disk, the density in the ring becomes ~ 10 times larger. Accumulation of matter near r_m and formation of a ring in the inner regions of the disk was also reported by GWB97, GBW99, and MS97, but these simulations were for non-stationary conditions.

For $r \lesssim r_m$ matter moves upward, away from the equatorial plane and goes into the funnel flow. The FF is formed after about one period of rotation $(T \sim 1)$ and is a stable feature during the length of the run, T = 50. Figure 5 shows the $\tilde{\beta} = 1$ line (black line). The base of the FF coincides with $r = r_m$; that is FF starts in the area where the magnetic stress is equal to the matter stress. This is observed in many other cases with different parameters (see §4 & §5). This is in accord with theories developed in 1970's (PR72, GL79a,b). We investigate the physics of FFs in §6.

Matter from the outer region of the disk $r > r_{br}$ tends to accrete inward. Often accretion rate is enhanced in the region where magnetic field has larger radial component B_r and hence stronger magnetic braking.

The accretion rate of matter from the region of the disk outside the ring varies with time. Consequently, the density in the inner ring and in the funnel flows also varies with time (Figure 5). When more matter accumulates in the ring, then the base of the FF is closer to the star, and the magnetospheric radius is smaller. For example, at T=10 (panel b of Figure 5), $r_m=0.92$; at T=30 (panel c) $r_m=1.2$. Subsequently, for T>50, even more matter came from the disk owing to viscosity, and the FF moved even closer to the star. A stationary state for T>50 may exist but at smaller values of α , $\alpha < 0.02$.

3.2. Simulations with Type II Initial Conditions

For Type II initial conditions, the inner radius of the disk is taken to be the corotation radius, $r_{cor} = 3$. The viscosity parameter is $\alpha = 0.02$, the same as in the abovementioned simulations. We were able of observe the evolution for more than 80 rotations of the inner radius of the disk. Figure 6 shows the evolution of the inner regions of the disk. We observed that the funnel flow did not form at the corotation radius as predicted in some theories (e.g., OS95). Instead, the disk slowly moves inward towards the star owing to the viscosity (see Figure 6). When the disk reached conditions where $\tilde{\beta} \approx 1$, the accreting matter goes up into the funnel flow. The FF formed after $T \approx 10$ rotations. At longer times, the structure of the disk and the FF are similar to those found for Type I initial conditions (Figure 5). But one difference is that for Type II initial conditions the inward motion of the inner edge of the disk drags the bases of magnetic loops inward, so that loops of the dipole are inclined to the disk. Such a situation is possible when the viscosity is larger than the diffusivity and magnetic flux in the disk accumulates closer to the star (e.g., S94, OS95), but the rest of the loop in the corona doesn't move so fast, so that the loops are inclined to the disk, and the B_r component is significant. When the magnetic field is inclined away from the axis of the disk, the magnetic force is much stronger than in case with no inclination (Lovelace, Berk & Contopoulos 1991, Oyed & Pudritz 1997; FE99, FE00). We observed opening of the magnetic field lines close to the magnetosphere. The opening was followed by reconnection, and subsequent opening. The process was quasi-periodic with a quasi-period $T \approx 3.5$ days. We also observed quasiperiodic oscillations of the inner radius of the disk between radii: $0.7 < r_m < 1.2$. The nature of the oscillations is the following: (1) First, the loop is stretched and the magnetic field "blocks" the path of matter to the FF. (2) Next, reconnection releases the stress, and matter accretes through the FF. (3) The new loop starts to stretch, and the process repeats. Figure 10 shows the quasi-periodicity of the accretion rate. These oscillations resemble those observed by GWB97 and GBW99, but on a much smaller scale. H97 and MS97 also observed enhanced accretion after the reconnection of elongated magnetic field lines near the magnetosphere. This work supports the idea of Aly & Kuijpers (1990) who proposed this mechanism of quasiperiodic oscillations.

We tested the dependence of the results on the viscosity for both types of initial conditions for $\alpha=0.01$ and $\alpha=0$. We obtained similar results, but the FF formed at slightly larger distances r as a result of smaller accretion

rate. Simulations with initial conditions of Types I and II have shown examples of possible situations which can be realized in nature. In the remainder of the paper we use the Type I initial conditions, because the FF starts earlier in this case.

3.3. Angular Momentum Transport

How is angular momentum transported between the disk and the star? Does the star spin-up or spin-down? In this section we analyze these questions using the run described in §3.1.

3.3.1. Angular Velocity of the Disk

We observed that the magnetic field lines which are responsible for the partial destruction of the disk at radii $r < r_{br}$ are also involved in the transport of angular momentum between the star and the disk. The magnetic filed lines connecting the star and the disk decrease the disk's angular velocity in a significant part of the braking region. Figure 7 shows the radial distribution of the angular velocities at different times. One can see that the angular velocity of the disk is significantly smaller than the Keplerian value in a broad region r < 1.3-1.8. We introduce the radius r_{Ψ} , such that for $r < r_{\Psi}$ the magnetic force on the disk is strong enough to cause a significant deviation from Keplerian rotation. The radius r_{Ψ} depends strongly on the accretion rate and varies between $r_{\Psi} \approx 1.8$ at T = 30, (when the inner disk is of low density) and $r_{\Psi} \approx 1$ at T = 10 (when the inner disk is dense).

Figure 8 shows the spatial distribution of the angular velocity, $\omega(R,\theta)$. One can see that for $r < r_{br} \approx 3$ the regions of constant angular velocity $\omega(R,\theta) = \text{const.}$ almost coincide with the regions of constant magnetic flux Ψ . Thus, the magnetic field line crossing the disk at radius r rotates in the corona with angular velocity $\omega(r)$. This is because most of the corona is matter-dominated, $\tilde{\beta} > 1$ (see black line in Figure 5), and the disk determines the rotation of the magnetic field lines. Magnetic field lines which cross the disk in the magnetically-dominated area (in the FF) rotate with the angular velocity of the star.

3.3.2. Spin Evolution of the Star

An important question is the angular momentum flux to the star. To answer this question, we calculated the flux of angular momentum (about the z-axis) carried by the matter \dot{L}_m and that carried by the 'twist' of the magnetic field \dot{L}_f ,

$$\dot{L}_m = \int \mathbf{dS} \cdot \rho r v_{\phi} \mathbf{v}_p \; , \quad \dot{L}_f = -\int \mathbf{dS} \cdot r B_{\phi} \mathbf{B}_p / 4\pi \; ,$$

evaluated at the surface of the star. In addition, we calculated accretion rate to the star, $\dot{M} = \int d\mathbf{S} \cdot \rho \mathbf{v}$.

Figure 9 shows the different fluxes as a function of time. Most of the angular momentum flux at the star is carried by the magnetic field; matter carries only $\sim 1\%$ of the total flux. The flux \dot{L}_f is positive so that it acts to *spin-up*

Fig. 14.— Disk-star interaction in case of "torqueless" accretion at $\Omega_* = 0.54$ and $r_{cor} = 1.5$ ($P_* = 3.3$ days for the T Tauri parameters of §2.2). Contour lines of magnetic flux Ψ are exponentially spaced between 0.07 and 0.7. These values of Ψ are smaller than those in Figure 11 because density at the inner edge of the disk is smaller and disk stops at smaller values of Ψ .

the star. The flux \dot{L}_f correlates with \dot{M} because incoming matter from distances $\sim r_m$ is responsible for bringing in positive angular momentum. At distances $r \sim r_m$ the angular momentum flux is carried mainly by the matter. These results partially confirm the hypothesis of S94, OS95, Li et al. (1996) that matter should carry little angular momentum as it approaches the star. However, our results indicate that this does not lead to the "torqueless" accretion predicted by these authors, because the angular momentum flux carried by the matter is transferred to a flux carried by the magnetic field with decreasing distance from the star. The small twist of the magnetic field near the star, $|B_{\phi}|/B_p \sim 0.1$ (see §6), is sufficient to carry the observed angular momentum transport flux (see discussion by Wang 1997).

From our simulations we find that the magnetic field lines responsible for spin-up or spin-down of the star pass through the disk at distances $r < r_{\Psi}$. Consequently the spin evolution of the star depends on the location of the corotation radius r_{cor} relative to r_{Ψ} . A star may spin-up, spin-down, or be in the regime of the "torqueless" accretion (see §4.2). For the case considered in this subsection of a slowly rotating star $r_{cor} = 3$, the star spins-up.

4. ACCRETION TO RAPIDLY ROTATING STARS

We performed a set of simulations for different angular velocities of the star Ω_* . Simulations were done for Type I initial conditions and with viscosity $\alpha=0.01$. The grid was $N_R \times N_\theta = 100 \times 51$ corresponding to the smaller region $R_{max} = 10$. The fastest rotation considered was such that at $r_{cor} = 1$, $\Omega_* = 1$ which corresponds to a rotation period $P_0 = 1.8$ days for the T Tauri parameters of §2.2. (The conversion formulae for dimensional period is $P_* = 1.8/\Omega_*$ days). In this section we discuss the dependence of the spin-up/spin-down rate of the star on Ω_* .

4.1. Rapidly Rotating Star: Spin-Down

Here we discuss the case of a rapidly rotating star, $\Omega_* = 1$, $r_{cor} = 1$ ($P_* = 1.8$ days), where $r_{cor} \approx r_m$. We observed that initially the accretion disk moved outward because the magnetic field of the star transferred its angular momentum to the disk. Later, for T > 3 the disk started to move inward towards the star, and finally a funnel flow formed (see Figure 11). In this case the thickness of the inner part of the disk is larger than that in the case of slowly rotating star, and matter accretes preferentially along the top layers of the disk.

Figure 12 shows the observed fluxes of matter and angular momenta to the star. Note, that the flux of an angular momentum is carried mainly by the magnetic field, \dot{L}_f , which is negative so that the star spins down. Thus, we

observe that as matter *accretes* to the star angular momentum flows out from the star. As in the case of slowly rotating star, we observe a correlation between the matter and angular momentum fluxes.

4.2. What is the Value of Ω_* for Torqueless Accretion?

We arranged a set of simulations to test if a particular value of Ω_* gives "torqueless" accretion. According to GL79b, at some angular velocity of the star Ω_{crit} , positive magnetic torque associated with the region $r < r_{cor}$ cancels the negative magnetic torque associated with the region $r > r_{cor}$ and the star can accrete without changing its angular momentum.

We performed simulations at different Ω_* (corresponding to $r_{cor} = 1.2, 1.3, 1.4, 1.5, 1.7, 2, 3, and 10$ and observed, that for $\Omega_* \approx 0.54 \, (r_{cor} = 1.5)$ the angular momentum flux L wanders back and forth around zero (see Figure 13). That is, it is positive for some time ($\sim 10P_0$), then becomes negative for a similar length of time, and then become positive again. We conclude that this Ω_* corresponds to torqueless accretion. The explanation for torqueless accretion was proposed in the 1970s (e.g., GL79b). Namely, when more matter is supplied to the disk, the magnetospheric radius r_m moves closer to the star, and as a result there is a positive angular momentum flux to the star. When less matter accretes, the magnetospheric radius r_m moves outward, and the flux of angular momentum is negative. Figure 14 shows the evolution of the density and poloidal magnetic field for times corresponding to positive angular momentum flux to the star (left panels), zero angular momentum flux (middle panels) and negative angular momentum flux (right panels). The variations of the accretion rate may be connected with accumulation of matter at $r \sim r_{br}$ where in this case $r_{br} \approx 3 - 3.5$ and subsequent accretion through instabilities.

The ratio of the corotation radius r_{cor} to the magnetospheric radius r_m is of general interest. At the moments when the torque is zero, $\dot{L}=0$ (see Figure 13), the magnetospheric radius had the following values: at T=24, $r_m=1$; at T=35, $r_m=1.07$; at T=46, $r_m=1.1$. That is, for $\dot{L}=0$ the ratio is: $r_{cor}/r_m\approx 1.4-1.5$. For similar simulations for faster rotation of the star $\Omega_*=0.67$ ($r_{cor}=1.3$), the angular momentum flux also wandered around zero value (see Figure 15), but most of time it was negative so that the star spins down. For simulations with more slowly rotating stars or larger corotation radii, $r_{cor}>1.5$, ($r_{cor}=1.7$, 2, 3, & 10), we observed that the star spins up.

5. DEPENDENCE ON THE STELLAR MAGNETIC FIELD

Fig. 15.— Same as on Figure 9, but $\Omega_* = 0.67$, $r_{cor} = 1.3$ ($P_0 = 2.7$ days for the T Tauri parameters of §2.2). The dot-dashed line corresponds to \dot{L}_m . The star spins down most of the time.

Fig. 16.— Disk-star interaction at different magnetic momenta of the star μ after T=10 rotations. Density (background) changes from $\rho=2.5$ (black) to $\rho=0.004$ (white) Magnetic flux Ψ (solid lines) is zero at panel a, and has limits: $\Psi=0.1-0.6$ on other panels.

Fig. 17.— Close view of a quasi-stationary funnel flow calculated for Type I initial conditions. The color background represents the logarithm of the density. The density has a minimum value $\rho = 0.004$ (blue) and a maximum value $\rho = 2$ (red). The lines are poloidal magnetic field lines or equivalently $\Psi(r,z) = \text{const}$ lines. The arrows represent the poloidal mass flux density $\rho \mathbf{v}$. The bold dark line is the field line approximately in the middle of the funnel flow. The variation of different quantities along this field line are shown in subsequent figures.

We did simulation runs for different magnetic moments, $\mu = 0$, 0.21, 0.42, 0.63 and 1.1, with other parameters fixed, $\Omega_* = 0.19$ ($r_{cor} = 3$), and $\alpha = 0.01$. At T = 0 the inner radius at of the disk was at r = 1 in all cases. The grid was similar to the one used in §4.

Figure 16 shows result after T=10 rotations. One can see that at smaller values of μ , the inner radius of the disk and FF are settled closer to the star than in the case of larger μ . In all cases, we observed that the base of the FF approximately coincides with the magnetosphere radius r_m , but at smaller μ this radius is smaller in accord with equation (11).

In case of even smaller μ the direct accretion to the surface of the star is observed, like in simulations by HSM96 and in some simulations by MS97.

The cases with stronger magnetic moment $\mu = 1.1, 0.63$ are more appropriate for explanation of T Tauri stars, because the gap between the star and the disk is comparable or larger than the radius of the star. At smaller magnetic momenta $\mu = 0.42, 0.21$, the gap is too small.

6. PHYSICS OF FUNNEL FLOWS

Here, we discuss the physics of a typical funnel flow, the case of a slowly rotating star with $r_{cor}=3$ (§3) after T=30 rotations. The specific heat ratio is $\gamma=5/3$. Figure 17 shows an enlarged picture of the FF. We determined the variation of different parameters as a function of distance (s) from the surface of the star along a fiducial poloidal field line through the middle of the FF. This field line is shown by the thick black line in Figure 17. Figures 18 – 21 show the variation of different parameters along this field line. Figure 18 shows that the density ρ and pressure P decrease along the FF, then increase again near the surface of the star. The temperature T initially varies slowly, but increases strongly approaching the star as a result of gas compression.

Figure 19 shows the variation of different velocities along the FF. Matter flows along the FF with poloidal velocity v_p . The velocity perpendicular to the poloidal magnetic field, v_q , is very small, $|v_q| << v_p$. The poloidal velocity v_p increases and becomes larger than the slow magnetosonic velocity c_{sm} at ~ 0.4 of the way. This point is expected to be closer to the disk in the case of cooler (and thinner) accretion disks (Koldoba et al. 2002). The flow become supersonic with the Mach number reaching $\mathcal{M} \approx 3.6$ at the surface of the star. Near the star, the poloidal velocity

is close to the free-fall velocity: $v_p \approx 0.7 v_{ff}$.

The poloidal velocity of the FF is much smaller than the Alfvén velocity v_A . The ratio decreases from $v_p/v_A \approx 1/3$ in the middle of the FF, to $v_p/v_A \approx 0.07$ at the star. Thus, the flow is strongly sub-Alfvénic. This validates the analysis of Koldoba *et al.* (2002) which proposed that the funnel flows were sub-Alfvénic.

It is important to understand the forces which drive matter out of the equatorial plane of the disk into the funnel flow, and which forces accelerate the flow towards the star. The force per unit mass F along the magnetic field line is obtained by multiplying the Euler equation by $\mathbf{B}_p/|\mathbf{B}_p|$. This gives

$$F = \omega^2 r \sin \chi - \frac{1}{\rho} \frac{\partial p}{\partial s} - \frac{\partial \Phi}{\partial s} - \frac{1}{8\pi \rho r^2} \frac{\partial (rB_\phi)^2}{\partial s} , \quad (12)$$

(Ustyugova et al. 1999), where χ is the angle of the field line to the z-axis. The terms on the right-hand-side represent the centrifugal force, the pressure gradient force, the gravitational force, and the magnetic force.

Figure 20 shows forces in the outer two-thirds of the poloidal path of the FF. We see that the pressure gradient force is responsible for driving matter up and out of the disk and into the funnel flow, while the gravitational force is responsible for the acceleration of matter in the rest of the FF. Note that the magnetic force in equation (12) is small and acts in the opposite direction. Thus, we did not observe the "magnetic levitation" force predicted by Li & Wilson (1999). We observed a finite B_{ϕ} field above the disk in the FF (see Figure 21), but the magnetic force is much smaller than the other forces and it is not sufficient to levitate matter above the disk.

Figure 21 shows that the angular velocity of the funnel flow decreases gradually from its value at the inner edge of the disk $(r=R_d)$ to a small negative value at the star. The negative value of ω at the star is due to the fact that the magnetic field has a small inclination in the direction of rotation of the star. For this reason matter moving along the magnetic field line comes to the star with an angular velocity less than Ω_* (see also Ghosh et al. 1977; Muzerolle et al. 2001).

Figure 21 shows the variation of the toroidal magnetic field along the funnel flow. The twisting of the dipolar field is relatively small with the "twist" $\gamma_{\phi} \equiv |B_{\phi}|/B_p < 0.15$. At the star, $\gamma_{\phi} \approx 0.04$. This is in accord with estimations by Wang (1997), who has shown that the twist near

the star should be small, but not a zero. Away from the funnel flow $|B_{\phi}|$ is of the order of B_p . We never observed conditions where $|B_{\phi}| >> B_z$ (discussed, e.g., by GL79a and Agapitou & Papaloizou 2000). The reason is that for $|B_{\phi}| >> B_p$, a torsional Alfvén wave forms and propagates outward into the corona where it dissipates.

In reality, matter may accrete through the magnetosphere owing to 3D instabilities, for example, the Rayleigh-Taylor or Kelvin-Helmholtz instability (Arons & Lea 1976a,b, Spruit & Taam 1990). Realistic investigations of the role of these instabilities is possible with 3D MHD simulations.

7. OPENING OF CORONAL MAGNETIC FIELD AND OUTFLOWS

In our simulations we observed coronal magnetic field lines at large distances from the star opening due to the initial differential rotation. Closer to the star the field lines were mostly closed, contrary to the predictions by Aly (1986), LRBK95 (see also Newman, Newman, & Lovelace 1992; Livio & Pringle 1992; Lynden-Bell & Boily 1994; Mikić & Linker 1994, Amari et al. 1996; FE99; FE00; Ustyugova et al 2000; Uzdenskyi, Königl & Litwin 2002). The difference in behavior can be explained as follows. The analytical or semi-analytical models suppose that the inertia of the of the matter is very small, $\beta = 8\pi p/B^2 \ll 1$, so that the plasma is in the "coronal" limit of Gold and Hoyle (1960). However, the inertia of the matter may be important. Romanova et al. (1998) simulated the dynamics of magnetic loops in the corona of a differentially rotating disk where $\beta \sim 1$. They observed that in the magnetically dominated regions (β < 1) the magnetic loops opened whereas in the matter-dominated regions ($\beta > 1$) the loops did not open.

The energy-density of the dipole field decreases rapidly with distance ($\sim R^{-6}$) compared with the matter energy-density in our simulations which varies slowly within the computational region. For this reason the magnetically-dominated region is restricted to a relatively small volume, R < 1-1.5, around the star (see black line at Figure 5). To overcome this feature of the dipole field, GWB97 and GBW99 adopted a rapid fall-off of density in the corona, $\rho \sim R^{-4}$. For this dependence the region of small β is greatly expanded and opening of the magnetic field is favored.

In order to investigate possible stronger outflows, we chose parameters so as to increase the region of magnetically-dominated corona. The magnetic moment was increased 5 times, $\mu=5.3$ (which corresponds to a magnetic field B=5.3 kG at the surface of the star). The density in the corona was decreased 3 times, $\rho_c=0.003$. This led to a higher Alfvén speed near the star, so that we increased the inner radius $R_{min}=0.8$ to cover the region of high Alfvén velocity, and increased the resolution of the grid to $N_R \times N_\theta = 120 \times 71$. We have $\tilde{\beta}=1$ at $r=R_d=1$ as in the other runs described in this work. The magnetic field is stronger and the initial density in the disk is about

10 times higher than in other simulations.

Figure 22 shows the results of the simulations. We observed that magnetic braking led to accretion of the inner part of the disk with velocity $v_r \approx 0.01 - 0.1$. Thus matter in the disk concentrated in a dense ring with $\rho \sim 10-14$. The disk angular velocity is significantly smaller than the Keplerian value but larger than the angular velocity of the star, $\Omega_* = 0.19$, which is a result of the interaction with the strong stellar magnetic field. A significant region above the corona corotates with the disk. Analysis of forces, similar to that of §6 shows that in the region r < 2, the centrifugal force drives matter along the magnetic field lines, but the force is not strong enough to open the magnetic field lines and matter accretes to the star forming multiple funnel flows (see Figure 22). However, the outer magnetic field lines, which are located at the edge of the magnetically-dominated region, become gradually open owing to combination of centrifugal and magnetic forces. Matter accelerates along the region of open field lines up to velocities $v \sim 0.5 v_{esc}$, where v_{esc} is the escape velocity. We anticipate that if the density in the corona decreases faster than in our model, then matter will outflow from the region. The observed matter and angular momentum fluxes of outflowing matter are small.

This test simulation provides evidence of how outflows can be formed from the disk in the quasi-stationary regime. Subsequent research is needed in this direction at different distributions of density of matter in the corona.

8. APPLICATION TO T TAURI STARS

Our simulations are well suited for modelling funnel flows to T Tauri stars because the entire flow can be well resolved. In the observed systems, the ratio of the inner radius of the disk where the FF begins to the stellar radius is $R_d/R_* \sim 2-4$. Such conditions are realized in our simulations.

The detailed nature of the magnetic fields of T Tauri stars is not known, and the fields may differ significantly from a dipole field (e.g., Safier 1998). However, recent spectral studies of T Tauri stars show broad emission lines which give evidence of matter inflow with nearly free-fall velocities (e.g., Hartmann et al. 1994; Lamzin, et al. 1996; Muzerolle et al. 2001). Such velocities may be easily explained in the model where matter inflows supersonically in a funnel flow along a dipolar field.

In the following we perform numerical estimates for the funnel flow to a typical T Tauri star using conversion scheme of §2.1. We assume the inner radius of the disk is $R_0=2.8R_*$, the star's mass $M_{0.8}\equiv M/(0.8M_\odot)$, its radius $R_2\equiv R/(2R_\odot)$, and its surface magnetic field $B_3=B/(10^3~{\rm G})$. Using these values we can derive reference values for the different physical variables. For the flow velocity, $v_0=(GM/R_0)^{1/2}\approx 1.63\times 10^7 M_{0.8}^{1/2}R_2^{-1/2}~{\rm cm/s}$. For the period of rotation at $r=R_0$, $P_0=2\pi R_0/v_0\approx 1.78~M_{0.8}^{-1/2}R_2^{3/2}$ days. For the density, $\rho_0=B_0^2/v_0^2\approx 6.93\times 10^{-12}B_3^2R_2M_{0.8}^{-1}~{\rm g/cm^{-3}}$. For the accretion rate,

Fig. 19.— Variation of different velocities with distance s along the fiducial magnetic field shown in Figure 17. v_p is the poloidal velocity (bold line), v_q is the velocity perpendicular to the magnetic field line, c_{sm} and c_{fm} are the slow and fast magnetosonic velocities, v_{ff} is a local free-fall velocity. The dashed line shows the Mach number \mathcal{M} .

Fig. 20.— Forces parallel to the flow as a function of distance s from the star's surface along the fiducial field line in Figure 17. Only part ($\sim 2/3$) of length of the flow is shown in order to resolve the forces acting near the disk. These forces are responsible for driving matter into the funnel flow. F_G is the gravitational force, F_C the centrifugal force, F_P the pressure gradient force, F_M the magnetic force, and F_R is the resultant force (bold line).

Fig. 21.— Angular velocity ω and the "twist" $|B_{\phi}|/B_p$ as a function of distance s from the star's surface along the bold field line in Figure 17.

Fig. 22.— Density and poloidal magnetic field lines for a case with outflows. The magnetic moment of the star $\mu=5.3$ is 5 times larger than that used in most of our simulations. The density in the corona is 3 times smaller than in other simulations. Color background represents the density, white solid lines - contours of magnetic flux, black solid line is the line $\tilde{\beta}=1$. Level lines of density are exponentially distributed between the minimum, $\rho=4\times10^{-4}$, and the maximum, $\rho=17.6$ values. The Ψ lines are exponentially distributed between $\Psi=0.1$ and $\Psi=3$. Arrows are velocities. The grid used was $N_R\times N_\theta=110\times71$, and the viscosity parameter was $\alpha=0.01$.

 $\dot{M}_0 = \rho_0 v_0 R_0^2 \approx 2.8 \times 10^{-7} B_3^2 M_{0.8}^{-1/2} R_2^{5/2} {\rm M}_{\odot}/{\rm year}$. For the temperature of the corona, $T_0 \approx 1.07 \times 10^6 M_{0.8} R_2^{-1} {\rm K}$.

In the following we calculate the different physical variables along the middle of the funnel flow shown in Figure 17. From Figure 19 the matter reaches a maximum poloidal velocity $v_{p*} \approx 277$ km/s at the star's surface, which is 79% of the free-fall velocity $v_{ff} \approx 350 \text{ km/s}$. The funnel flow will of course give a distribution of velocities along the line of sight to a distant observer. The smallest line of sight velocities are for matter immediately above the disk where the speeds are $\sim 10\%$ of v_{p*} . The line of sight velocity distribution is important for the interpretation of observed spectral lines (e.g., Folha and Emerson 2001). The poloidal velocity is $\sim 1/3$ the Alfvén velocity v_A above the disk (at $s \approx 1$) and decreases to $v_p \approx v_A/15$ at the star's surface. The velocity across the magnetic field lines v_q is very small (see Figure 19). Thus, matter flows along the magnetic field. The flow become supersonic above the disk and the Mach number reaches $\mathcal{M} \approx 3.6$ at the surface of the disk.

The initial density of matter in the disk at R_0 is $\rho_0 \approx 6.9 \times 10^{-12} \ \rm gcm^{-3}$, and the density of matter in the FF (see Figure 18) varies in the range $(1.2-9.2)\times 10^{-12} \ \rm cm^{-3}$ which is typical for T Tauri stars. Our typical accretion rate to the star through the FF is $\dot{M} \sim (0.6-1.2)\times 10^{-7} \ \rm M_{\odot}/year$, which agrees with estimates for T Tauri stars (Hartmann *et al.* 1998). The initial temperature in the disk is $T\approx 9.6\times 10^3$ K which is several times higher than expected in the disks of T Tauri stars at R_0 . As mentioned earlier this higher temperature is needed to give adequate resolution in the vertical direction through the disk. We observed that matter in the FF was heated by adiabatic compression to higher temperatures, $T\sim 1.2\times 10^5$ K.

The fact that we use "free" boundary conditions at the surface of the star means that we cannot account for the stand-off shock at the stellar surface, surface heating, and other physical phenomena close to the star. Study of these processes can be done with a separate set of simulations.

The investigated quasi-stationary funnel flows correspond to Classical T Tauri stars (CTTS) (see Hartman 1998) where variability is not strong and possible outflows are weak. Previous simulations of very fast accretion with subsequent strong outflows were done by HSM96, MS97, H97, GWB97, and GBW99, and these may corre-

spond to earlier stages of evolution of young stellar objects (YSOs of classes 0 and I) which show evidence of episodic non-stationary accretion (e.g., FU Orionis type stars) and strong outflows (e.g. HH30). Non-stationary accretion may be initiated by thermal instability (Lightman & Eardley 1974) or by global magnetic instability of the disk (Lovelace, Romanova, & Newman 1994; Lovelace, Newman, & Romanova 1997), or by tidal interaction with a binary companion (Larson 2002).

9. CONCLUSIONS

9.1. Funnel Flows

We have done a wide range of MHD simulations of disk accretion to a rotating aligned dipole in order to understand the different accretion phenomena. The simulations show that funnel flows (FF), where matter flows out of the disk plane and essentially free-falls along the stellar magnetic field lines, are a robust feature of disk accretion to a dipole. Specifically, we find that

- (1). The disk truncates and a funnel flow forms near the magnetosphere radius r_m , where magnetic pressure of the dipole is comparable to the kinetic plus thermal pressure of the disk matter.
- (2). The velocity of matter in the FF is much smaller than the Alfvén velocity, $|\mathbf{v}| \sim (0.05-0.3)v_A$, so that matter flows along the magnetic field lines. The funnel flow accelerates and become supersonic. The Mach number is $\mathcal{M} \approx 3-4$ at the surface of the star. At the star velocity is close to the free-fall velocity: $v_p \approx 0.7v_{ff}$.
- (3). The angular velocity of the FF gradually varies from its value at the inner edge of the disk to the angular velocity of the star. The 'twist' of the magnetic field lines in the FF is small, $|B_{\phi}|/B_{p} < 0.1$, and it has a maximum approximately in the middle of the FF.
- (4). The main forces which are responsible for dragging matter to the FF are matter pressure gradient force (near the disk) and gravitational force in the rest of the FF. Magnetic force is negligibly small.
- (5). About 1/3 of the magnetic flux responsible for the spin-up/spin-down the star goes through the FF, while the remainder is above the FF.

Regarding the interaction between the disk and the star we find that

- (1) The magnetic field of the star influences the nearby regions of the disk inside a radius r_{br} , while viscosity dominates at larger radii. The radius r_{br} depends on magnetic moment of the star μ and density in the disk.
- (2). Inside the radius r_{br} the disk is strongly inhomogeneous. The density is 2-3 times smaller than in the disk without magnetic field. Magnetically braked matter accumulates near magnetosphere and forms a dense ring and funnel flow.
- (3). The star may spin-up or spin-down depending on the ratio of its rotation rate to the rotation rate at the inner radius of the disk. We find that "torqueless" accretion is possible when $r_{cor}/r_m \approx 1.5$, where r_{cor} is the corotation radius.
- (4). At the star's surface, the angular momentum flux is transported mainly by the 'twist' of the magnetic field. Angular momentum carried by matter in the disk at $\sim r_m$ is transferred almost completely to the magnetic field at the star's surface.
- The coronal magnetic field is observed to open and close, but strong outflows were not observed for the considered parameters and quasi-equilibrium initial conditions. In the area of the disk where the field is strong,

- $r < r_{\Psi} \approx 0.5 r_{br}$, the magnetic field lines tend to decelerate/accelerate rotation of the disk instead of being opened. Besides, opening of magnetic field loops is suppressed by matter dominated corona compared to GBW99 who accepted dependence $\rho \sim R^{-4}$.
- (6). Strong outflows may be associated with strongly non-stationary accretion in the disk as observed in simulations by HSM96, MS97, and H97 or when the disk is very dense and magnetic field lines are inclined to the disk as in simulations by FE99, FE00. Alternatively the outflows may occur in cases where the density of the corona decreases sufficiently rapidly with distance as in the simulations by GWB97 and GBW99. Sporadic outflows can arise from a global magnetic instability of the disk (e.g., Lovelace et al. 1994, 1997, 2002), but they may be absent during the quiescent evolution of the disk-star system.

This work was supported in part by NASA grant NAG5-9047, by NSF grant AST-9986936. RMM thanks NSF POWRE grant for partial support. RVEL was partially supported by grant NAG5-9735, GVU and AVK were partially supported by INTAS grant and by Russian program "Astronomy." The authors thank the referees for numerous comments and suggestions.

REFERENCES

Agapitou, V., & Papaloizou, J.C.B. 2000, MNRAS, 317, 273 Aly, J.J. 1985, A&A, 143, 19

Aly, J.J., & Kuijpers, J. 1990, A&A, 227, 473 Amari, T., Luciani, J.F., Aly, J.J., & Tagger, M. 1996, ApJ, 466,

Arons, J., & Lea, S.M. 1976a, ApJ, 207, 914

Arons, J., & Lea, S.M. 1976b, ApJ, 210, 792 Balbus, S.A., & Hawley, J.F. 1991, ApJ, 376, 214 Bardou, A., & Heyvaerts, J. 1996, A&A, 307, 1009

Bildsten, L., Chakrabarty, D., Chiu, J., Finger, M.H., Koh, D.T., Nelson, R.W., Prince, T.A., Rubin, B.C., Scott, D.M., Stollberg, M., Vaughan, B.A., Wilson, C.A., Wilson, R.B. 1997, ApJ Supplement, 113, 367

Bisnovatyi-Kogan, G.S., & Ruzmaikin, A.A. 1976, Astrophys. Space Sci., 42, 401

Brandenburg, A., & Campbell, C.G. 1998, MNRAS, 298, 223 Camenzind, M. 1990 in: Rev. Mod. Astron. 3, ed. G. Klare, Springer-Verlag (Heidelberg), 234 Davidson, K. & Ostriker, J.P. 1973, ApJ, 179, 585 Edwards, S., Hartigan, P., Ghandour, L., & Andrulis, L. 1994, AJ,

Elstner, D., & Rüdiger, G. 2000, Astron. Astrophys., 358, 612 Feigelson, E.D., & DeCampli, W.M. 1981, ApJ, 243, L89 Feigelson, E.D., & Montmerle, T. 1999, Ann. Rev. Astron. Astro-

Feigelson, E.D., & Montmerle, T. 1999, Ann. Rev. Astron. Astrophys., 37, 363
Fendt, C., Camenzind, M., & Appl, S. 1995, A&A, 300, 791
Fendt, C., & Elstner, D. 1999, Astron. Astrophys. 349, L61 (FE99)
Fendt, C., & Elstner, D. 2000, Astron. Astrophys. 363, 208 (FE00)
Foha, D.F.M., & Emerson, J.P. A&A, 365, 90
Gold, T., & Hoyle, F. 1960, MNRAS, 120, 7
Ghosh, P., Lamb, F.K., & Pethick, C.J. 1977, ApJ, 217, 578
Ghosh, P., & Lamb, F.K. 1979, ApJ, 232, 259 (GL79a)
Ghosh, P., & Lamb, F.K. 1979, ApJ, 234, 296 (GL79b)
Gold, T., & Hoyle, F. 1960, MNRAS, 120, 89
Goodson, A.P., Winglee, R., & Böhm, K.H. 1997, ApJ, 489, 199

(GWB97)

Goodson, A.P., & Winglee, R. 1999, ApJ, 524, 159 Goodson, A.P., Böhm, K.H., & Winglee, R. 1999, ApJ, 524, 142 (GBW99)

Hartmann, L., Calvet, N., Gullbring, E., & D'Alessio, P. 1998, ApJ, 495, 385

Hartmann, L., Accretion Processes in Star Formation, Cambridge University Press, 1998

Hartmann, L., Hewett, R., & Calvet, N., 1994, ApJ, 426, 669 Hayashi, M.R., Shibata, K., & Matsumoto, R. 1996, ApJ, 468, L37 (HSM96)

Hirose, S., Uchida, Y., Shibata, K., Matsumoto, R. 1997, PASJ, 49,

Koldoba, Á.V., Kuznetzov, O.A., & Ustyugova, G.V. 1992, Report of the Keldysh Institute of Applied Mathematics of the Russian Academy of Science, No. 69

Koldoba, A.V., Lovelace, R.V.E, Ustyugova, G.V., & Romanova,

M.M. 2002, Astronomical Journal, 123, 2019 Koldoba, A.V., & Ustyugova, G.V. 1994, Report of the Keldysh Institute of Applied Mathematics of the Russian Academy of Science, No. 87

ence, No. 87
Königl, A. 1991, ApJ, 370, L39
Lamb, F.K., Pethick, C.J., & Pines, D. 1973, ApJ, 184, 271
Lamzin, S.A., Bisnovatyi-Kogan, G.S., Errico, L., Giovannelli, F.,
Katysheva, N.A., Rossi, C., & Vittone, A.A. 1996, A&A, 306, 877
Larson, R.B. 2002, MNRAS, 332, 155
Li, J., & Wilson, G. 1999, ApJ, 527, 910
Li, J., Wickramasinghe, D.T., & Ruediger, G. 1996, ApJ, 469, 765
Li, J., & Wickramasinghe, D.T. 1998, MNRAS, 300, 1015
Lightman, A.P. & Fardley, D.M. 1974, ApJ, 187, L1

Lightman, A.P., & Eardley, D.M. 1974, ApJ, 187, L1 Livio, M. & Pringle, J.E. 1992, MNRAS, 259, 23P

Lovelace, R.V.E., Berk, H.L., & Contopoulos, J. 1991, ApJ, 379,

Lovelace, R.V.E., Romanova, M.M., & Newman, W.I. 1994, ApJ, 437, 136

Lovelace, R.V.E., Newman, W.I., & Romanova, M.M. 1997, ApJ, 484, 628

Lovelace, R.V.E., Li, H., Koldoba, A.V., Ustyugova, G.V., & Romanova, M.M. 2002, ApJ, in press

Lovelace, R.V.E., Romanova, M.M., & Bisnovatyi-Kogan, G.S. 1995, MNRAS, 275, 244 (LRBK95)
Lynden-Bell, D., & Boily, C. 1994, MNRAS, 267, 146
Mikić, Z., & Linker, J.A. 1994, ApJ, 430, 898

Miller, K.A. & Stone, J.M. 1997, ApJ, 489, 890 (MS97) Muzerolle, J, Calvet, N., & Hartmann, L. 2001, ApJ, 550, 944 Newman, W.I., Newman, A.L, & Lovelace, R.V.E. 1992, ApJ, 392,

Ostriker, E.C., & Shu, F.H. 1995, ApJ, 447, 813 (OS95) Ouyed, R., & Pudritz, R.E. 1997, ApJ, 482, 712 Pagtz, G., & Camenzind, M. 1996, Astron. Astrophys., 308, 77

(FC90) Pringle, J.E. & Rees, M.J. 1972, A&A, 21, 1P (PR72) Romanova, M.M., Ustyugova, G.V., Koldoba, A.V., Chechetkin, V.M., & Lovelace, R.V.E. 1998, ApJ, 500, 703 Ryu, D., Jones, T.W., & Frank, A. 1995, ApJ, 252, 785

Shakura, N.I., & Sunyaev, R.A. 1973, Astron. & Astrophys., 24, 337 Scharlemann, E.T. 1978, ApJ, 219, 617

Shu, F.H., Najita, J., Ruden, S.P., & Lizano, S. 1994, ApJ, 429, 797

Ostriker, E.C., & Shu, F.H. 1995, ApJ, 447, 813
Safier, P.N. 1998, ApJ, 494, 336
Spruit, H.C., & Taam, R.E. 1990, Astron. & Astrophysics, 229, 475
Stone, J.M., Hawley, J.F., Gammie, C.F., Balbus, S.A. 1996, ApJ, 463, 656

Ustyugova, G.V., Koldoba, A.V., Romanova, M.M., Chechetkin, V.M., & Lovelace, R.V.E. 1995, ApJ, 439, L39

Ustyugova, G.V., Koldoba, A.V., Romanova, M.M., Chechetkin, V.M., & Lovelace, R.V.E. 1999, ApJ, 516, 221
Ustyugova, G.V., Lovelace, R.V.E., Romanova, M.M., Li, H., Colgate, S.A. 2000, ApJ, 541, L21
Uzdensky, D.A., Königl, A., & Litwin, C. 2002, ApJ, 565, 1205
Wang, Y.-M. 1995, ApJ, 449, L153
Wang, Y.-M. 1997, ApJ, 487, L85
Warner, B. 1995, Cataclysmic Variable Stars (Cambridge: Cambridge Univ. Press)

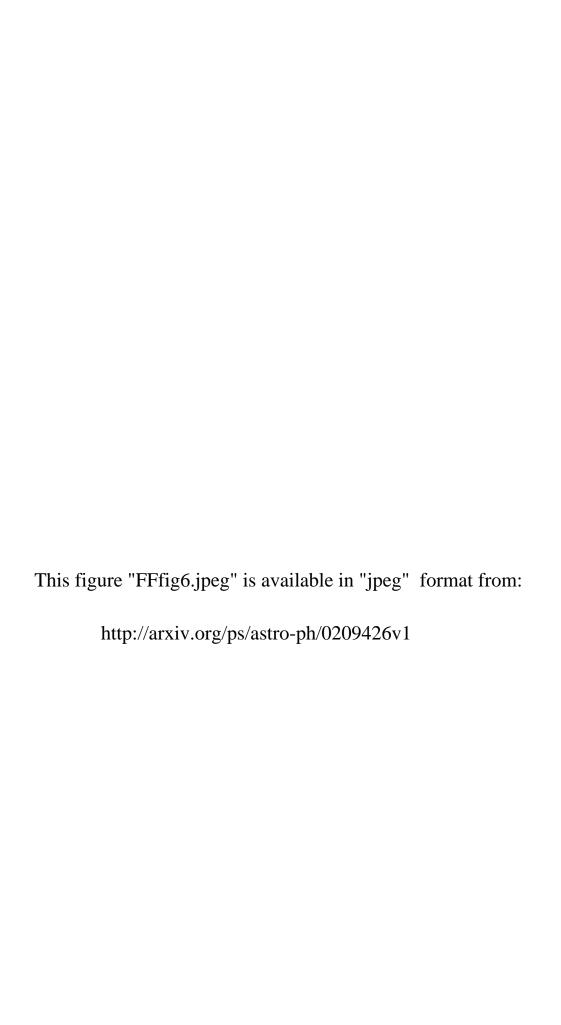
This figure "FFfig1.jpeg" is available in "jpeg" format from: http://arxiv.org/ps/astro-ph/0209426v1

This figure "FFfig2.jpeg" is available in "jpeg" format from:

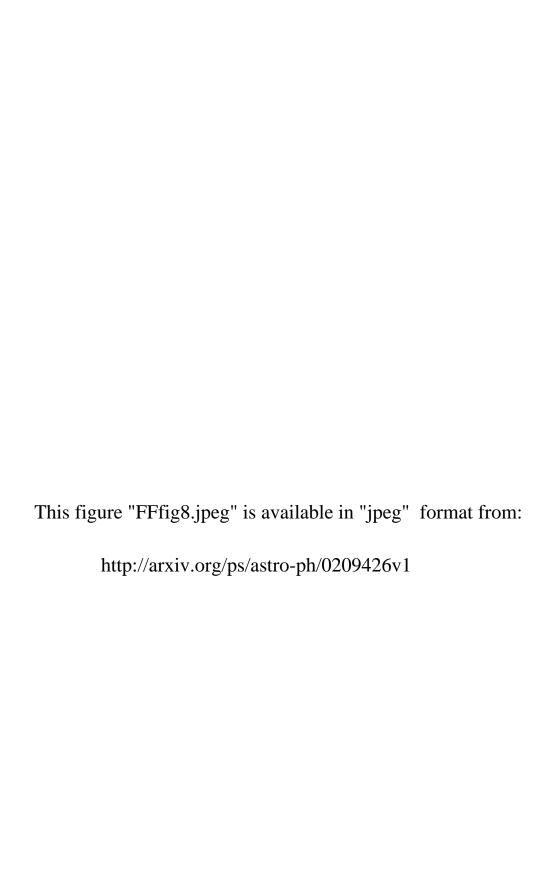
This figure "FFfig3.jpeg" is available in "jpeg" format from:

This figure "FFfig4.jpeg" is available in "jpeg" format from: http://arxiv.org/ps/astro-ph/0209426v1

This figure "FFfig5.jpeg" is available in "jpeg" format from: http://arxiv.org/ps/astro-ph/0209426v1



This figure "FFfig7.jpeg" is available in "jpeg" format from:



This figure "FFfig9.jpeg" is available in "jpeg" format from: http://arxiv.org/ps/astro-ph/0209426v1

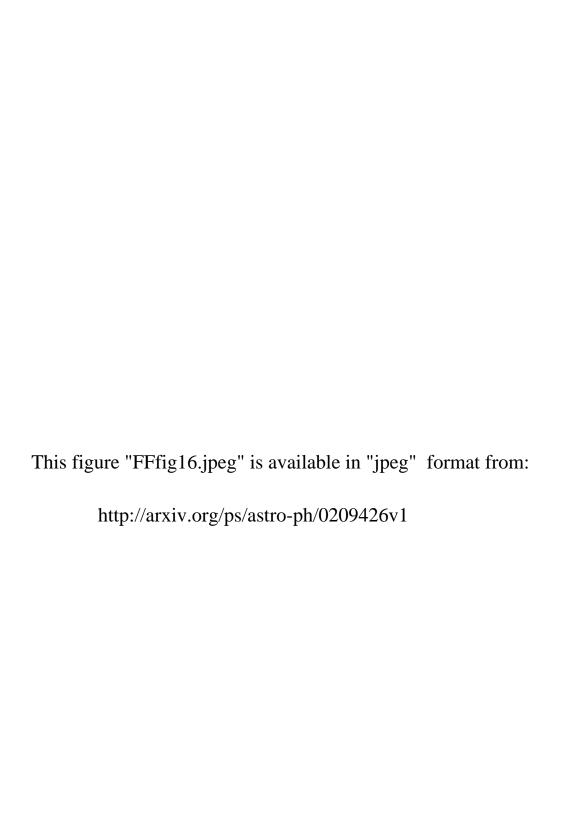
This figure "FFfig10.jpeg" is available in "jpeg" format from: http://arxiv.org/ps/astro-ph/0209426v1

This figure "FFfig11.jpeg" is available in "jpeg" format from: http://arxiv.org/ps/astro-ph/0209426v1

This figure "FFfig12.jpeg" is available in "jpeg" format from:

This figure "FFfig13.jpeg" is available in "jpeg" format from:

This figure "FFfig14.jpeg" is available in "jpeg" format from: http://arxiv.org/ps/astro-ph/0209426v1 This figure "FFfig15.jpeg" is available in "jpeg" format from: http://arxiv.org/ps/astro-ph/0209426v1



This figure "FFfig17.jpeg" is available in "jpeg" format from: http://arxiv.org/ps/astro-ph/0209426v1

This figure "FFfig18.jpeg" is available in "jpeg" format from: http://arxiv.org/ps/astro-ph/0209426v1

This figure "FFfig19.jpeg" is available in "jpeg" format from: http://arxiv.org/ps/astro-ph/0209426v1

This figure "FFfig20.jpeg" is available in "jpeg" format from: http://arxiv.org/ps/astro-ph/0209426v1

This figure "FFfig21.jpeg" is available in "jpeg" format from:

This figure "FFfig22.jpeg" is available in "jpeg" format from: